Invariant Filtering for Full-State Estimation of Ground Robots in Non-Inertial Environments

Author Names Omitted for Anonymous Review. Paper-ID [add your ID here]

Abstract*—This paper presents an invariant extended Kalman filter (InEKF) approach for estimating the relative pose and linear velocity of ground robots—either legged or wheeled—using an inertial measurement unit (IMU) attached to the robot, encoders, and an external IMU placed on the moving ground. The approach explicitly accounts for ground motion in non-inertial environments, such as ships or airplanes, where the ground rotates or accelerates in the inertial frame. Unlike previous methods, it does not rely on known ground pose. This consideration introduces complexity due to the nonlinear dynamics and kinematics of the reference frame. Despite this complexity, the proposed filter, based on the InEKF methodology, includes a process model that partially satisfies the group affine condition. The leg odometry-based measurement model meets the right-invariant observation form for deterministic scenarios, though the wheel odometry model does not. Observability analysis demonstrates that all state variables are observable during a broad range of ground motions, overcoming the partial observability limitations of previous filters. Experiments on a Digit humanoid robot and a Jackal wheeled robot verify the filter's effectiveness across various ground motions. *This manuscript summarizes our paper [9] that has been accepted by the IEEE/ASME Transactions on Mechatronics.

I. Introduction

Wheeled and legged robots have shown impressive locomotion and manipulation capabilities in stationary environments [14]. Researchers are now deploying them in non-inertial settings (e.g., shipboards and airplanes [10, 11, 12, 15, 18]) for tasks such as emergency response and maintenance, where continuous ground motion relative to the inertial frame presents significant challenges for accurate real-time state estimation [5].

Existing state estimators address inertial measurement unit (IMU) integration drift by fusing it with encoder, camera, LiDAR, or GPS data [6, 20], often using the standard extended Kalman filters (EKF) [3]. Yet, EKFs rely on inaccurate system linearization, causing slow convergence under significant errors. The invariant extended Kalman filter (InEKF) overcomes this by ensuring trajectory-independent linearization under group affine and invariant observation conditions, achieving accurate estimation even with significant errors [1].

InEKF is widely used for estimating wheeled and legged locomotor states on stationary ground [7, 17, 23]. To address non-zero contact area velocity caused by slippage, visual-inertial odometry [13, 19] measures body velocity in the world frame, but exteroceptive sensors (e.g., cameras and LiDAR) struggle to detect landmarks in non-inertial environments including enclosed ship spaces. Furthermore, [22] uses an autoregressive model to address slippage, and [2] treats slippage-induced measurements as outliers during filter updates. However, both approaches are designed for static ground, and ignoring persistent ground motion can cause substantial uncertainty that degrades performance.

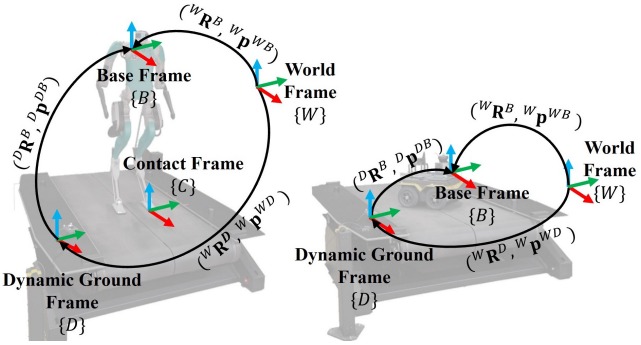

Fig. 1: Illustration of the reference frames and variables of interests to this study. The reference frames fixed to the robot base, contact points, dynamic ground, and inertial world frame are denoted as $\{B\}$, $\{C\}$, $\{D\}$, and $\{W\}$, respectively. The treadmill serves as a dynamic ground that can rotate and translate in the inertial world frame.

Recently, the static-ground assumption has been relaxed to account for ground motion [4], using accurate knowledge of the ground's absolute pose and velocity in the inertial frame. Yet, such knowledge is often unavailable in practical applications. Beyond locomotion in non-inertial environments, state estimation in non-inertial frames is also relevant in settings where multiple robots move relative to each other. These systems rely on sensors such as ultra-wideband modules [16] and cameras [21], integrated with IMU data to estimate relative pose and velocity. Still, slow sampling rates of these sensors may not be suitable for real-time control and planning. Estimating a robot's pose and motion relative to the non-inertial ground frame is essential in environments where the ground undergoes dynamic motion, such as ships or airplanes.

This paper presents an InEKF that accurately estimates a ground robot's relative pose and linear motion with respect to a non-inertial ground frame. The main contributions of this work are: **(a)** analytical extension of the InEKF approach to apply to both legged and wheeled robots, significantly enhancing its general applicability; **(b)** expansion of the wheel-odometry-based measurement model to non-inertial environments and formulating the leg-odometry-based model into a right-invariant observation form; **(c)** derivation of a closed-form discretized process model for real-world implementation; **(d)** observability analysis that examines the effects of ground motions and reveals full state observability under general ground motion conditions; and **(e)** experimental validation on legged and wheeled robots on a pitch and sway treadmill.

II. Methodology

A. State Representation

Following the notations in Fig. 1, ${}^{W}\mathbf{R}_t^B$, ${}^{W}\mathbf{v}_t^{WB}$, and ${}^{W}\mathbf{p}_t^{WB}$ denote the robot's absolute orientation, velocity, and position with respect to the world frame $\{W\}$, respectively. Similarly, ${}^{W}\mathbf{R}_t^D$, ${}^{W}\mathbf{v}_t^{WD}$, and ${}^{W}\mathbf{p}_t^{WD}$ represent the absolute orientation, linear velocity, and position of the dynamic ground frame $\{D\}$ with respect to $\{W\}$, respectively. The relative orientation and position of the robot's base frame $\{B\}$ with respect to $\{D\}$ are denoted as ${}^{D}\mathbf{R}_t^B$ and ${}^{D}\mathbf{p}_t^{DB}$, respectively.

Then, the relative base orientation $\mathbf{R}_t$, velocity $\mathbf{v}_t$, and position $\mathbf{p}_t$ are defined and related to the absolute ones as:

$$\begin{aligned}\mathbf{R}_t &:= {}^{D}\mathbf{R}_t^B = ({}^{W}\mathbf{R}_t^D)^{\mathsf{T}}{}^{W}\mathbf{R}_t^B,\\ \mathbf{v}_t &:= ({}^{W}\mathbf{R}_t^D)^{\mathsf{T}}({}^{W}\mathbf{v}_t^{WB} - {}^{W}\mathbf{v}_t^{WD}),\\ \mathbf{p}_t &:= {}^{D}\mathbf{p}_t^{DB} = ({}^{W}\mathbf{R}_t^D)^{\mathsf{T}}({}^{W}\mathbf{p}_t^{WB} - {}^{W}\mathbf{p}_t^{WD}),\end{aligned} \tag{1}$$

where ${}^{W}\mathbf{v}_t^{WB} = \frac{d}{dt}({}^{W}\mathbf{p}_t^{WB})$ and ${}^{W}\mathbf{v}_t^{WD} = \frac{d}{dt}({}^{W}\mathbf{p}_t^{WD})$.

Additionally, we include the position of the contact frame $\{C\}$'s origin, denoted as $\mathbf{d}_t := {}^{D}\mathbf{p}_t^{DC}$, as a state variable to account for potential foot slippage on the dynamic ground.

By the InEKF methodology [1], the state is expressed as:

$$\mathbf{X}_t := \begin{bmatrix}\mathbf{R}_t & \mathbf{v}_t & \mathbf{p}_t & \mathbf{d}_t\\ \mathbf{0}_{1,3} & 1 & 0 & 0\\ \mathbf{0}_{1,3} & 0 & 1 & 0\\ \mathbf{0}_{1,3} & 0 & 0 & 1\end{bmatrix} \in \mathcal{G}, \tag{2}$$

where $\mathcal{G}$ is $SE_3(3)$, an extension of $SE(3)$.

B. Process Model

The proposed filter uses standard, low-cost sensors: (a) an IMU mounted on the robot's base/torso (gyroscope + accelerometer), (b) joint encoders for joint angles/velocities measurements, and (c) an external IMU placed arbitrarily on the dynamic ground. As in previous filter designs [3, 7], we build the process model based on IMU motion dynamics, due to its accuracy and simplicity. The novelty of the proposed modeling lies in the formulation of the *relative* IMU motion dynamics within the non-inertial ground frame.

1) Absolute IMU motion dynamics: The input $\mathbf{u}_t$ of the process model consists of the IMU readings ${}^{i}\tilde{\boldsymbol{\omega}}_t^{Wi}$ and ${}^{i}\tilde{\mathbf{a}}_t^{Wi}$ with $i \in \{B, D\}$. These are measurements of the true angular velocity ${}^{i}\boldsymbol{\omega}_t^{Wi}$ and specific force ${}^{i}\mathbf{a}_t^{Wi}$ of the reference frame $\{i\}$ relative to the world frame $\{W\}$, expressed in the frame $\{i\}$, respectively. Corrupted by white Gaussian zero-mean noise ${}^{i}\mathbf{w}_t^{\omega}$ and ${}^{i}\mathbf{w}_t^{a}$, these readings are expressed as: ${}^{i}\tilde{\boldsymbol{\omega}}_t^{Wi} = {}^{i}\boldsymbol{\omega}_t^{Wi} + {}^{i}\mathbf{w}_t^{\omega}$ and ${}^{i}\tilde{\mathbf{a}}_t^{Wi} = {}^{i}\mathbf{a}_t^{Wi} + {}^{i}\mathbf{w}_t^{a}$.

The input $\mathbf{u}_t$ is then defined as: $\mathbf{u}_t = [{}^{B}\tilde{\boldsymbol{\omega}}_t^{\mathsf{T}}, {}^{B}\tilde{\mathbf{a}}_t^{\mathsf{T}}, {}^{D}\tilde{\boldsymbol{\omega}}_t^{\mathsf{T}}, {}^{D}\tilde{\mathbf{a}}_t^{\mathsf{T}}]^{\mathsf{T}} := [({}^{B}\tilde{\boldsymbol{\omega}}_t^{WB})^{\mathsf{T}}, ({}^{B}\tilde{\mathbf{a}}_t^{WB})^{\mathsf{T}}, ({}^{D}\tilde{\boldsymbol{\omega}}_t^{WD})^{\mathsf{T}}, ({}^{D}\tilde{\mathbf{a}}_t^{WD})^{\mathsf{T}}]^{\mathsf{T}}$.

Based on the rigid body dynamics of an IMU frame, the absolute IMU motion dynamics are given as [7]: $\frac{d}{dt}\left({}^{W}\mathbf{R}_t^i\right) = {}^{W}\mathbf{R}_t^i[{}^{i}\tilde{\boldsymbol{\omega}}_t - {}^{i}\mathbf{w}_t^{\omega}]_\times$, $\frac{d}{dt}\left({}^{W}\mathbf{v}_t^{Wi}\right) = {}^{W}\mathbf{R}_t^i\left({}^{i}\tilde{\mathbf{a}}_t - {}^{i}\mathbf{w}_t^{a}\right) + \mathbf{g}$, and $\frac{d}{dt}\left({}^{W}\mathbf{p}_t^{Wi}\right) = {}^{W}\mathbf{v}_t^{Wi}$, where $\mathbf{g}$ is the gravitational acceleration.

2) Relative IMU motion dynamics: To estimate the pose $(\mathbf{R}_t, \mathbf{p}_t)$ and velocity $\mathbf{v}_t$ relative to the dynamic ground, their dynamic models are used as the process model.

Taking the time derivative of both sides of (1) and substituting the absolute IMU motion dynamics into the resulting equation, we derive the dynamic models of $\mathbf{R}_t$, $\mathbf{v}_t$, and $\mathbf{p}_t$ as:

$$\begin{aligned}\tfrac{d}{dt}\mathbf{R}_t &= \mathbf{R}_t\left[{}^{B}\tilde{\boldsymbol{\omega}}_t - {}^{B}\mathbf{w}_t^{\omega}\right]_\times - \left[{}^{D}\tilde{\boldsymbol{\omega}}_t - {}^{D}\mathbf{w}_t^{\omega}\right]_\times \mathbf{R}_t,\\ \tfrac{d}{dt}\mathbf{v}_t &= -\left[{}^{D}\tilde{\boldsymbol{\omega}}_t - {}^{D}\mathbf{w}_t^{\omega}\right]_\times \mathbf{v}_t + \mathbf{R}_t\left({}^{B}\tilde{\mathbf{a}}_t - {}^{B}\mathbf{w}_t^{a}\right)\\ &\quad - \left({}^{D}\tilde{\mathbf{a}}_t - {}^{D}\mathbf{w}_t^{a}\right),\\ \tfrac{d}{dt}\mathbf{p}_t &= -\left[{}^{D}\tilde{\boldsymbol{\omega}}_t - {}^{D}\mathbf{w}_t^{\omega}\right]_\times \mathbf{p}_t + \mathbf{v}_t.\end{aligned} \tag{3}$$

3) Contact point dynamics: When no contact-point slippage occurs, the contact velocity $\frac{d}{dt}\mathbf{d}_t$ is zero with respect to the ground frame $\{D\}$. To model potential slippage, the contact velocity in $\{D\}$, expressed in the contact frame $\{C\}$, is treated as white Gaussian noise ${}^{C}\mathbf{w}_t^{v}$. Then, the dynamics of the relative contact position $\mathbf{d}_t$ is expressed as:

$$\tfrac{d}{dt}\mathbf{d}_t = \mathbf{R}_t\mathbf{s}_R(\tilde{\mathbf{q}}_t)(-{}^{C}\mathbf{w}_t^{v}), \tag{4}$$

where $\mathbf{s}_R$ is the robot's forward kinematics for the contact-frame orientation relative to the base frame $\{B\}$ and $\tilde{\mathbf{q}}_t$ is the joint angles measured by encoders.

4) Proposed process model: The process model in (3) and (4) can be compactly expressed as:

$$\tfrac{d}{dt}\mathbf{X}_t = f_{u_t}(\mathbf{X}_t) + ({}^{D}\mathbf{w}_t)^{\wedge}\mathbf{X}_t - \mathbf{X}_t({}^{B}\mathbf{w}_t)^{\wedge}, \tag{5}$$

where ${}^{D}\mathbf{w}_t := [({}^{D}\mathbf{w}_t^{\omega})^{\mathsf{T}}, ({}^{D}\mathbf{w}_t^{a})^{\mathsf{T}}, \mathbf{0}_{1,6}]^{\mathsf{T}}$, ${}^{B}\mathbf{w}_t := [({}^{B}\mathbf{w}_t^{\omega})^{\mathsf{T}}, ({}^{B}\mathbf{w}_t^{a})^{\mathsf{T}}, \mathbf{0}_{1,3}, (\mathbf{s}_R(\tilde{\mathbf{q}}_t)\ (-{}^{C}\mathbf{w}_t^{v}))^{\mathsf{T}}]^{\mathsf{T}}$,

By InEKF theory [1], the deterministic portion of the process model in (3) is group affine [8], making the logarithmic error equations for relative pose and linear velocity trajectory-independent and exactly linear in the deterministic case. However, incorporating the dynamics of the relative contact position in (4) causes the full deterministic process model (5), $\frac{d}{dt}\mathbf{X}_t = f_{u_t}(\mathbf{X}_t)$, to lose the group affine property, invalidating these theoretical guarantees. Nonetheless, as shown in [7], an "imperfect InEKF" can still outperform the standard EKF.

C. Measurement Models

We use leg or wheel odometry to derive the measurement models for leveraging encoder data to correct state estimates. Due to differences in locomotion, separate models are developed for legged and wheeled robots. Unlike previous odometry-based models [3, 7], the proposed measurement model extends from static terrain to dynamic ground by formulating the model in the non-inertial ground frame.

1) Leg-odometry-based measurement model: Let $\mathbf{q}_t$ represent the robot's joint angles at time t, and denote $\mathbf{s}_p(\mathbf{q}_t)$ the forward kinematics function for the contact-point position relative to the base, expressed in the base frame. Based on the positional relationship between the base and contact point, we define the following leg-odometry-based measurement model:

$$\mathbf{R}_t^{\mathsf{T}}(\mathbf{d}_t - \mathbf{p}_t) = \mathbf{s}_p(\mathbf{q}_t). \tag{6}$$

Suppose that the encoder reading $\tilde{\mathbf{q}}_t$ is corrupted by additive white Gaussian noise $\mathbf{w}_t^q$ as $\tilde{\mathbf{q}}_t = \mathbf{q}_t + \mathbf{w}_t^q$. Then, we can obtain the first-order approximation of $\mathbf{s}_p(\mathbf{q})$ as $\mathbf{s}_p(\tilde{\mathbf{q}}_t - \mathbf{w}_t^q) \approx \mathbf{s}_p(\tilde{\mathbf{q}}_t) - \frac{\partial \mathbf{s}_p}{\partial \mathbf{q}}(\tilde{\mathbf{q}}_t)\mathbf{w}_t^q$.

By the theory of InEKF, the proposed measurement model in (6) meets the following right-invariant observation form:

$$\mathbf{Y}_t = \mathbf{X}_t^{-1}\mathbf{b}_t + \mathbf{n}_t^{\text{Leg}}, \tag{7}$$

where $\mathbf{Y}_t := [\mathbf{s}_p^{\mathsf{T}}(\tilde{\mathbf{q}}_t), 0, 1, -1]^{\mathsf{T}}$, $\mathbf{b} := [\mathbf{0}_{1,4}, 1, -1]^{\mathsf{T}}$, and $\mathbf{n}_t^{\text{leg}} := [(\frac{\partial \mathbf{s}_p}{\partial \mathbf{q}}(\tilde{\mathbf{q}}_t)\mathbf{w}_t^q)^{\mathsf{T}}, \mathbf{0}_{1,3}]^{\mathsf{T}}$.

TABLE I: Observability analysis results under different ground motion conditions.

Ground motion conditions		Observable state variables
$\forall {}^D\tilde{\mathbf{a}}_t \in \mathbb{R}^3$	${}^D\tilde{\omega}_x \not\equiv 0, {}^D\tilde{\omega}_y \not\equiv 0, {}^D\tilde{\omega}_z \not\equiv 0\ \forall t$	$\mathbf{R}_t, \mathbf{v}_t, \mathbf{p}_t$ (*full observability*)
	${}^D\tilde{\omega}_x \not\equiv 0, {}^D\tilde{\omega}_y \not\equiv 0, {}^D\tilde{\omega}_z \equiv 0, \forall t$	
	${}^D\tilde{\omega}_x \not\equiv 0, {}^D\tilde{\omega}_y \equiv 0, {}^D\tilde{\omega}_z \not\equiv 0, \forall t$	
	${}^D\tilde{\omega}_x \equiv 0, {}^D\tilde{\omega}_y \not\equiv 0, {}^D\tilde{\omega}_z \not\equiv 0, \forall t$	
	${}^D\tilde{\omega}_x \not\equiv 0, {}^D\tilde{\omega}_y \equiv 0, {}^D\tilde{\omega}_z \equiv 0\ \forall t$	$\mathbf{R}_t, \mathbf{v}_t, \mathbf{p}_t$ except for p_x
	${}^D\tilde{\omega}_x \equiv 0, {}^D\tilde{\omega}_y \not\equiv 0, {}^D\tilde{\omega}_z \equiv 0, \forall t$	$\mathbf{R}_t, \mathbf{v}_t, \mathbf{p}_t$ except for p_y
	${}^D\tilde{\omega}_x \equiv 0, {}^D\tilde{\omega}_y \equiv 0, {}^D\tilde{\omega}_z \not\equiv 0, \forall t$	$\mathbf{R}_t, \mathbf{v}_t, \mathbf{p}_t$ except for p_z
${}^D\tilde{a}_x \not\equiv 0$ and/or ${}^D\tilde{a}_y \not\equiv 0, \forall t$; $\forall {}^D\tilde{a}_z \in \mathbb{R}$	${}^D\tilde{\boldsymbol{\omega}}_t \equiv \mathbf{0}_{3,1}, \forall t$	$\mathbf{R}_t, \mathbf{v}_t$
elsewhere		roll, pitch, $\mathbf{v}_t$

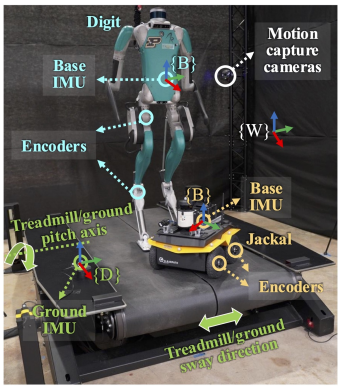

Fig. 2: Experimental setup includes a Digit robot, a Jackal robot, a treadmill (i.e., dynamic ground), an IMU mounted on the side plate of the treadmill's dynamic surface, and motion capture cameras.

This right-invariant observation property ensures that the log-error equation for the leg-odometry-based model is exactly linear and trajectory-independent in the deterministic case, enabling accurate covariance propagation, fast convergence, and high estimation accuracy despite significant errors [1].

2) Wheel-odometry-based measurement model: The derivation of the measurement model begins with building the relationship between the robot's base and contact-point positions: $\mathbf{d}_t - \mathbf{p}_t = \mathbf{R}_t {}^B\mathbf{p}_t^{BC}$, where ${}^B\mathbf{p}_t^{BC}$ is the contact frame $\{C\}$'s origin position with respect to the base frame $\{B\}$, which is a constant vector known from the robot's kinematics parameters. Taking the time derivative of both sides of this equation gives:

$$\tfrac{d}{dt}(\mathbf{d}_t - \mathbf{p}_t) = (\mathbf{R}_t[{}^B\boldsymbol{\omega}_t]_\times - [{}^D\boldsymbol{\omega}_t]_\times \mathbf{R}_t){}^B\mathbf{p}_t^{BC} + \mathbf{R}_t \tfrac{d}{dt}({}^B\mathbf{p}_t^{BC}). \tag{8}$$

When the robot's wheels roll on the dynamic ground without slippage, the contact-point velocity satisfies $\frac{d}{dt}(\mathbf{d}_t) = \mathbf{0}_{3,1}$.

Also, we consider the typical nonholonomic constraints of wheels rolling on a plane, where wheels can roll forward or backward but not vertically or laterally. Then, the direction of the robot's body/base velocity $\frac{d}{dt}({}^B\mathbf{p}_t^{CB})$, which is relative to the dynamic ground and expressed in the base frame $\{B\}$, is fixed in $\{B\}$. For simplicity, suppose that the base velocity $\frac{d}{dt}({}^B\mathbf{p}_t^{CB})$ is parallel to the x-axis of $\{B\}$.

The angular rates of the left and right wheels, measured by wheel encoders, are denoted as ω_t^{left} and ω_t^{right}, respectively, with positive values corresponding to the forward direction of $\frac{d}{dt}({}^B\mathbf{p}_t^{CB})$. Then, for a differential wheel robot without wheel slippage and under the nonholonomic constraints, the forward component of its base velocity $\frac{d}{dt}({}^B\mathbf{p}_t^{CB})$ is $\frac{1}{2}(r\omega^{\text{left}} + r\omega^{\text{right}})$ with r the wheel radius; that is, $\frac{d}{dt}({}^B\mathbf{p}_t^{BC}) = \left[-\frac{1}{2}(r\omega^{\text{left}} + r\omega^{\text{right}}), 0, 0\right]^\mathsf{T}$.

With $\frac{d}{dt}(\mathbf{d}_t) = \mathbf{0}_{3,1}$ and the expression of $\frac{d}{dt}({}^B\mathbf{p}_t^{BC})$, (8) becomes: $[{}^D\boldsymbol{\omega}_t]_\times \mathbf{p}_t - \mathbf{v}_t = (\mathbf{R}_t[{}^B\boldsymbol{\omega}_t]_\times - [{}^D\boldsymbol{\omega}_t]_\times \mathbf{R}_t){}^B\mathbf{p}_t^{BC} + \mathbf{R}_t \frac{d}{dt}({}^B\mathbf{p}_t^{BC})$. Considering uncertainties (e.g., wheel slippage and encoder noise), this measurement model is rewritten as:

$$\mathbf{y}_t = \mathbf{h}(\mathbf{X}_t) + \mathbf{n}_t^{\text{wheel}}, \tag{9}$$

where $\mathbf{y}_t = \left[-\frac{1}{2}(r\tilde{\omega}^{\text{left}} + r\tilde{\omega}^{\text{right}}), 0, 0\right]^\mathsf{T} + [{}^B\tilde{\boldsymbol{\omega}}_t]_\times {}^B\tilde{\mathbf{p}}_t^{BC}$, $\mathbf{h}(\mathbf{X}_t) = \mathbf{R}_t^\mathsf{T}([{}^D\tilde{\boldsymbol{\omega}}_t]_\times \mathbf{p}_t - \mathbf{v}_t + [{}^D\tilde{\boldsymbol{\omega}}_t]_\times \mathbf{R}_t {}^B\tilde{\mathbf{p}}_t^{BC})$, and $\mathbf{n}_t^{\text{wheel}}$ is the lumped white Gaussian noise induced by the uncertainties.

D. Observability Analysis

This section presents the observability analysis used to determine which state variables are observable under different ground motion conditions. The key results are summarized in Tab. I. In general, if at most one element of ${}^D\tilde{\boldsymbol{\omega}}_t$ is always zero while the other two are not, all state variables $\mathbf{R}_t$, $\mathbf{v}_t$, and $\mathbf{p}_t$ are *fully observable*. Additionally, if two elements of ${}^D\tilde{\boldsymbol{\omega}}_t$ are always zero while one is not, all velocity, orientation, and position variables are observable except for the position along the rotation axis corresponding to the nonzero element. For example, if only the pitch component of ${}^D\tilde{\boldsymbol{\omega}}_t$ is not always zero, all state variables are observable except for p_y (i.e., the base position along the y-axis of $\{D\}$).

Due to space constraints, detailed derivations and proofs have been omitted here; please refer to the full version of the paper for a comprehensive observability analysis and InEKF design [9].

III. Experimental Validation

A. Experimental Setup

Digit humanoid and Jackal wheeled robots are tested under static (RM1) and dynamic (RM2) motions. To evaluate the proposed filter under various ground motions, the following four treadmill pitch angle and sway displacement profiles are used: (**PITCH1**) $8^\circ \sin(\frac{2\pi}{3.5}t)$; (**PITCH2**) $5^\circ \sin(\frac{\pi}{2.8}t)$; (**SWAY1**): $5\cos(\frac{\pi}{2.5}t)$ (cm); and (**SWAY2**): $4\cos(\frac{\pi}{2.5}t)$ (cm). Digit is equipped with an onboard IMU attached to its torso/base and six encoders in each leg. An external IMU is mounted on the treadmill. A Vicon motion capture system (Fig. 2) provides ground truth for filter evaluation. To assess the observability analysis results under various combinations of ${}^D\tilde{\boldsymbol{\omega}}_t$ and ${}^D\tilde{\mathbf{a}}_t$, and to test the applicability of the proposed filter under different sensor placements, the external IMU is mounted on the treadmill at three different yaw angles relative to the treadmill surface: (**PLACEMENT1**) 0°; (**PLACEMENT2**) -20°; and (**PLACEMENT3**) 45°.

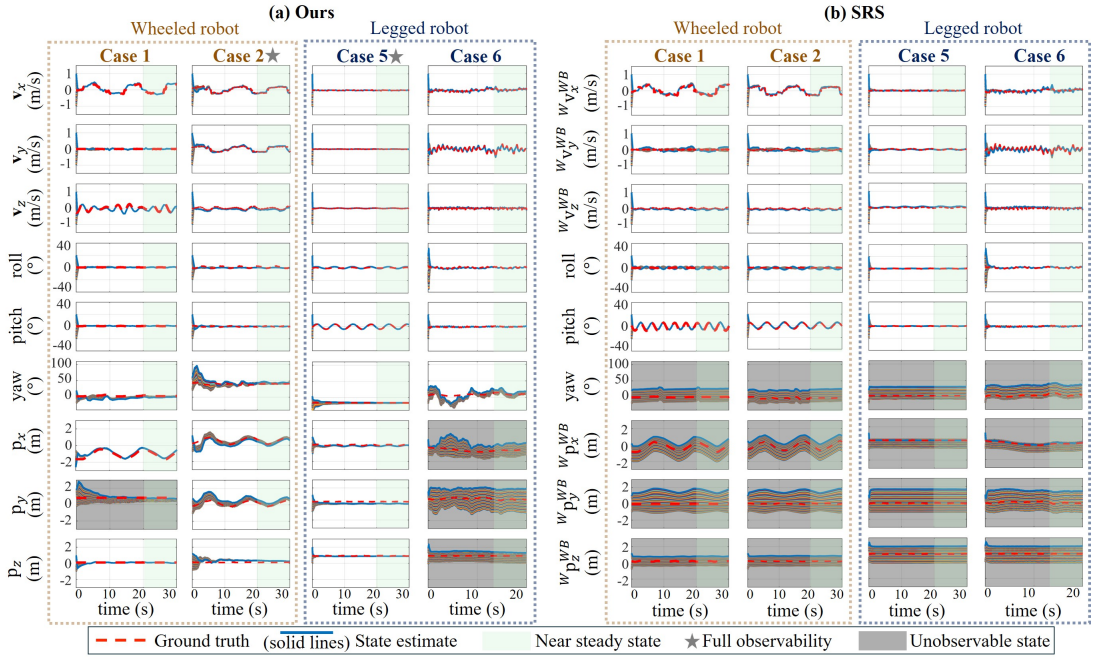

Fig. 3: Estimation results for the robot's relative base position, orientation, and linear velocity using the proposed filter, compared to the absolute estimates from the SRS filter, across four experiment cases. Here, the right subscript x, y, or z of a scalar indicates the corresponding x, y, or z element of the associated vector. For example, ${}^{W}p_x^{DB}$ represents the x-element of the position vector ${}^{W}\mathbf{p}^{DB}$.

TABLE II: Test cases with different robot and treadmill motions and IMU placements.

Robots	Test cases	Experiment conditions
Jackal	Case 1	RM2; PITCH1; PLACEMENT1
	Case 2	RM2; (PITCH1, SWAY1); PLACEMENT3
Digit	Case 5	RM1; (PITCH2, SWAY2); PLACEMENT2
	Case 6	RM2; SWAY2; PLACEMENT1

TABLE III: Final errors under our and the baseline SRS filters.

Test case	Base yaw (°) (Ours/SRS)	p_x (m) (Ours/SRS)	p_y (m) (Ours/SRS)	p_z (m) (Ours/SRS)
Case 1	1.41/12.28	0.10/0.60	0.35/0.78	0.04/0.37
Case 2	3.65/13.01	0.38/0.60	0.16/0.79	0.14/0.40
Case 5	2.12/12.25	0.17/0.34	0.26/0.86	0.04/0.66
Case 6	13.65/19.79	0.67/0.34	0.70/0.79	0.39/0.67

B. Results and Analysis

This subsection compares the experimental performance of the proposed and existing InEKF approaches for Cases 1, 2, 5, and 6 (Tab. II). Cases 3, 4, 7, and 8 are omitted due to space constraints. For the complete set of experimental results and analysis, please refer to the full version of the paper [9] and the experimental videos: https://youtu.be/jaqjfBX92ls.

1) Observability during different ground motions: The SRS filter estimates roll, pitch, and linear velocities but fails to recover yaw and position. In contrast, our filter ensures full observability when the ground angular velocity is non-zero along at least two axes (Cases 1, 2, 5). This is confirmed in Fig. 3-a), where our estimates closely match ground truth. Case 6, involving pure sway without rotation, leads to unobservable position states, consistent with our analysis.

2) Convergence Rate: For observable variables, both filters converge rapidly. However, the proposed filter converges faster, particularly for pitch and velocity, due to its right-invariant measurement model and explicit modeling of ground motion.

3) Final accuracy: Near steady-state ($t = 20$ s), both filters yield similar accuracy for observable states under mild motion (Cases 5, 6). Under aggressive motions (Cases 1, 2), SRS exhibits degraded lateral velocity and roll estimation. Our proposed filter maintains high accuracy across all cases. In fully observable scenarios, it accurately recovers yaw and position; see Table III. Errors increase for unobservable directions (e.g., p_x in Case 6), as expected.

IV. Conclusion

This paper introduced an InEKF approach for accurately estimating the relative pose and linear motion of legged and wheeled ground robots in non-inertial environments with accelerating or rotating ground. The filter's process and measurement models explicitly account for ground motions, relaxing the static-ground assumption of existing methods. Distinct from current filters, which offer only partial observability with IMUs and encoders, our approach ensures full-state observability under a general class of ground motions. Experimental results confirmed the filter's rapid convergence and high accuracy on legged and wheeled robots during various ground motions. Comparative studies further highlighted its advantage in achieving full observability.

References

[1] Axel Barrau and Silvère Bonnabel. The invariant extended Kalman filter as a stable observer. *IEEE Transs. Autom. Contr.*, 62(4):1797–1812, 2016.

[2] Michael Bloesch, Christian Gehring, Péter Fankhauser, Marco Hutter, Mark Hoepflinger, and Roland Siegwart.

State estimation for legged robots on unstable and slippery terrain. In *Proc. IEEE Int. Conf. Intel. Rob. Syst.*, pages 6058–6064, 2013. doi: 10.1109/IROS.2013.6697236.

[3] Michael Bloesch, Marco Hutter, Mark Hoepflinger, Stefan Leutenegger, Christian Gehring, C. Remy, and Roland Siegwart. State estimation for legged robots-consistent fusion of leg kinematics and IMU. *Rob.*, 17: 17–24, 2013.

[4] Yuan Gao, Chengzhi Yuan, and Yan Gu. Invariant filtering for legged humanoid locomotion on a dynamic rigid surface. *IEEE/ASME Trans. Mechatr.*, 27(4):1900–1909, 2022.

[5] Yuan Gao, Yukai Gong, Victor Paredes, Ayonga Hereid, and Yan Gu. Time-varying ALIP model and robust foot-placement control for underactuated bipedal robotic walking on a swaying rigid surface. In *Proc. Amer. Contr. Conf.*, pages 3282–3287, 2023.

[6] Patrick Geneva, Kevin Eckenhoff, Woosik Lee, Yulin Yang, and Guoquan Huang. Openvins: A research platform for visual-inertial estimation. In *Proc. IEEE-RAS Int. Conf. Rob. Autom.*, pages 4666–4672, 2020.

[7] Ross Hartley, Maani Ghaffari, Ryan M Eustice, and Jessy W Grizzle. Contact-aided invariant extended Kalman filtering for robot state estimation. *Int. J. Rob. Res.*, 39(4):402–430, 2020.

[8] Zijian He, Sangli Teng, Tzu-Yuan Lin, Maani Ghaffari, and Yan Gu. Legged robot state estimation within non-inertial environments. In *Proc. IEEE Contr. Dec. Conf.*, 2024, in press.

[9] Zijian He, Sangli Teng, Tzu-Yuan Lin, Maani Ghaffari, and Yan Gu. Invariant filtering for full-state estimation of ground robots in non-inertial environments. https://www.thetracelab.com/uploads/1/1/3/0/113094493/he2025tmech.pdf, 2025. Accessed: May 31, 2025.

[10] Amir Iqbal, Yuan Gao, and Yan Gu. Provably stabilizing controllers for quadrupedal robot locomotion on dynamic rigid platforms. *IEEE/ASME Trans. Mechatr.*, 25(4): 2035–2044, 2020.

[11] Amir Iqbal, Sushant Veer, and Yan Gu. Asymptotic stabilization of aperiodic trajectories of a hybrid-linear inverted pendulum walking on a vertically moving surface. In *Proc. Amer. Contr. Conf.*, pages 3030–3035, 2023.

[12] Amir Iqbal, Sushant Veer, and Yan Gu. Analytical solution to a time-varying LIP model for quadrupedal walking on a vertically oscillating surface. *Mechatr.*, 96: 103073, 2023.

[13] Yeeun Kim, Byeongho Yu, Eungchang Mason Lee, Joonha Kim, Hae-Won Park, and Hyun Myung. STEP: State estimator for legged robots using a preintegrated foot velocity factor. *IEEE Rob. Autom. L.*, 7(2):4456–4463, 2022.

[14] Joonho Lee, Marko Bjelonic, Alexander Reske, Lorenz Wellhausen, Takahiro Miki, and Marco Hutter. Learning robust autonomous navigation and locomotion for wheeled-legged robots. *Sc. Rob.*, 9(89):eadi9641, 2024.

[15] Stephen Misenti, Brendan Hertel, Bowen Weng, Ryan Donald, Advait Jawaji, Magnus-Tryggvi Kosoko-Thoroddsen, J Gregory Trafton, Adam Norton, Reza Azadeh, and Yan Gu. Experimental evaluation of commercial quadruped robots: stability and performance in non-inertial environments. *Int. J. Intel. Rob. Appl.*, pages 1–26, 2025.

[16] Mohammed Ayman Shalaby, Charles Champagne Cossette, Jerome Le Ny, and James Richard Forbes. Multi-robot relative pose estimation and IMU preintegration using passive UWB transceivers. *IEEE Trans. Rob.*, 2024.

[17] Pengcheng Shi, Zhikai Zhu, Shiying Sun, Xiaoguang Zhao, and Min Tan. Invariant extended Kalman filtering for tightly coupled lidar-inertial odometry and mapping. *IEEE/ASME Trans. Mechatr.*, 28(4):2213–2224, 2023.

[18] Jacob Stewart, I Chang, Yan Gu, and Petros A Ioannou. Adaptive ankle torque control for bipedal humanoid walking on surfaces with unknown horizontal and vertical motion. In *Proc. Amer. Contr. Conf.*, 2024, in press.

[19] Sangli Teng, Mark Mueller, and Koushil Sreenath. Legged robot state estimation in slippery environments using invariant extended Kalman filter. In *Proc. IEEE Int. Conf. Rob. Aut.*, pages 3104–3110, 2021.

[20] David Wisth, Marco Camurri, and Maurice Fallon. Vilens: Visual, inertial, lidar, and leg odometry for all-terrain legged robots. *IEEE Trans. on Rob.*, 39(1):309–326, 2022.

[21] Zhiren Xun, Jian Huang, Zhehan Li, Zhenjun Ying, Yingjian Wang, Chao Xu, Fei Gao, and Yanjun Cao. CREPES: Cooperative relative pose estimation system. *arXiv preprint arXiv:2302.01036*, 2023.

[22] Xihang Yu, Sangli Teng, Theodor Chakhachiro, Wenzhe Tong, Tingjun Li, Tzu-Yuan Lin, Sarah Koehler, Manuel Ahumada, Jeffrey M Walls, and Maani Ghaffari. Fully proprioceptive slip-velocity-aware state estimation for mobile robots via invariant Kalman filtering and disturbance observer. In *Proc. IEEE Int. Conf. Intel. Rob. Syst.*, pages 8096–8103, 2023.

[23] Zenan Zhu, Seyed Mostafa Rezayat Sorkhabadi, Yan Gu, and Wenlong Zhang. Design and evaluation of an invariant extended Kalman filter for trunk motion estimation with sensor misalignment. *IEEE/ASME Trans. Mechatr.*, 27(4):2158–2167, 2022.